Original article

The effect of matrix-fracture permeability contrast on hydrocarbon foam performance in oil-wet carbonate

Magda Ibrahim Youssif, Keerti Vardhan Sharma[ID]*, Lamia Goual, Mohammad Piri

Center of Innovation for Flow through Porous Media, Department of Energy and Petroleum Engineering, University of Wyoming, Laramie 82071, USA

Abstract:
Foam-based enhanced oil recovery methods are becoming instrumental in increasing hydrocarbon production from unconventional reservoirs. However, the efficacy of such techniques is significantly affected by reservoir heterogeneity and adverse wettability conditions. This experimental study addresses such challenges by investigating the effect of fracture-matrix permeability contrast on the effectiveness of foam-based enhanced oil recovery in fractured oil-wet porous systems under reservoir conditions. Fractured oil-wet Minnesota Northern Cream Buff carbonate core samples were employed and fracture permeability was varied using four different mixtures of proppants with varying mesh sizes. An amphoteric surfactant was used as the foaming agent and the aqueous solution was prepared in a synthetic brine of 200,000 ppm salinity. The results showed that foam reduced gas mobility in fractures, diverting gas to the matrix and mobilizing oil toward fractures. The permeability of the fracture showed a significant impact on foam behavior in oil-wet porous systems. It was noted that as the fracture-matrix permeability contrast decreased to a certain ratio, the apparent viscosity of the foam increased, resulting in the enhancement of fracture-matrix interactions and, therefore, higher oil recovery. However, further reduction in this ratio resulted in a significant decline in foam strength. The optimal fracture-matrix permeability contrast was determined when using 100 wt.% of 100 mesh sand, enabling the creation of small and durable bubbles, which notably restricted gas movement and led to higher oil recovery. The results confirm that foam can be a viable and effective alternative to traditional gas injection methods in fractured carbonates with oil-wet characteristics.

1. Introduction

Naturally fractured carbonate reservoirs exhibit distinctive and irregular porosity and permeability distribution patterns, resulting in an anisotropic behavior (Dominguez, 1992; Van Golf-Racht, 1996; Fitch, 2011; Guerriero et al., 2013; Moore and Wade, 2013; Shafiei et al., 2018). These subsurface systems typically consist of carbonates, such as limestone and dolomite, and are known for their complex pore space properties (Burchette, 2012; Rashid et al., 2023). The heterogeneity caused by fractures in the formations significantly impacts fluid flow dynamics and hydrocarbon recovery efficiency. Such geological settings are classified into four categories (Types I to IV) based on their permeability and porosity (Allan and

Sun, 2003). Type I reservoirs exhibit minimal matrix porosity and permeability, relying primarily on fractures for storing and producing hydrocarbons. Type II has slightly improved matrix porosity and permeability compared to type I. In this case, the matrix provides some degree of storage capacity, while fractures function as the principal pathways for fluid flow. Type III reservoirs, often referred to as microporous, demonstrate high matrix porosity but low matrix permeability. In such systems, the matrix is primarily occupied by residing fluids, while fractures act as the channels for fluid movement across different zones of matrices. Finally, the Type IV counterparts, known as macroporous, are characterized by high matrix porosity and permeability. Within this category, the matrix contributes significantly to the storage capacity of the forma-
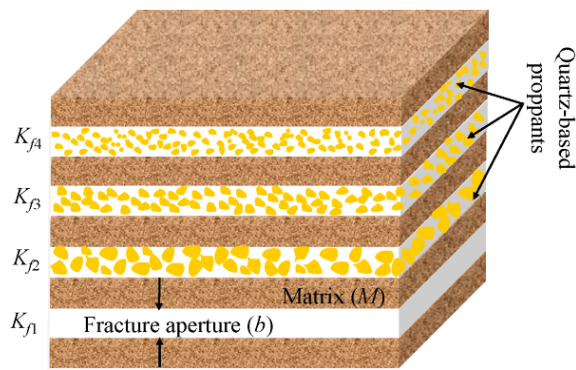
*Corresponding author.
E-mail address: msolima1@uwyo.edu (M. I. Youssif); ksharma1@uwyo.edu (K. V. Sharma); lgoual@uwyo.edu (L. Goual); mpiri@uwyo.edu (M. Piri).

Fig. 1. Schematic of proppant-packed and unpacked fracture systems in which the fracture permeability (K_f) of all distinct zones shows $K_{f1} > K_{f2} > K_{f3} > K_{f4}$.

tion as well as facilitating the flow through the pore space, whereas fractures mainly enhance the overall permeability.

The present study mainly focuses on Type II and III reservoirs in which the fracture-matrix interactions significantly influence the dynamics of fluid flow and hydrocarbon production from the tight matrices. The injection of water and gas in such formations results in negligible pressure gradients across the fractures due to early breakthroughs, leading to insignificant interactions between the fractures and matrices (Fernø, 2012). This phenomenon is manifested as poor sweep efficiency and low recovery rates (Davidson and Snowdon, 1978; Elfeel et al., 2016; Youssif et al., 2023).

Several new techniques have surfaced recently for enhanced oil recovery from fractured geological systems. The mechanisms associated with these methods can be divided into two categories, addressing conventional as well as fractured reservoirs. The first involves modifying the properties of rock formation and resident fluids using low-salinity water flooding (Park et al., 2018; Zaeri et al., 2018; Qin et al., 2019; Karimova et al., 2023) and injections of alkaline, surfactants (Chen and Mohanty, 2015; Janssen et al., 2019b; Dordzie and Dejam, 2021), polymers (Shedid, 2006; Sayedakram and Mamora, 2011; Sedaghat et al., 2013), and gas (Karimaie et al., 2008; Panfili and Cominelli, 2014; Sofla et al., 2016). These techniques mainly focus on improving oil mobility in conventional systems by changing the physical and chemical properties, including surface activity, solubility, density, viscosity, and composition. This results in increased production due to reduced interfacial tension, altered wettability, and inhibited gravity drainage and viscous fingering due to changed physicochemical properties of fluids. However, the performance of those utilizing specific chemicals and gases is marred by challenges such as high costs, mechanical trapping, chemical and thermal degradation, and lower recovery rates.

On the other hand, the second category of recovery mechanisms aims at enhancing the interactions between displacing and residing fluids in fractured reservoirs. It is achieved by regulating the petrophysical properties of fractures using proppants of specific sizes, shapes, and types (Liang et al., 2016; Youssif et al., 2023). They are crucial in maintaining fractures' aperture and conductivity (Liang et al., 2016) while reducing their permeability contrast to matrices, thereby improving the

viability of such interactions. Four different fracture arrangements are shown in Fig. 1, where each possesses certain properties of specific grain size distribution and layering of the proppants. The fracture-matrix permeability contrast ($PC_{F/M}$), defined as the ratio of permeabilities of the two, is remarkably high in open fractures, specifically with rough surfaces and no proppants. Introducing a monolayer of proppants diminishes the fracture permeability to a certain extent, reducing the $PC_{F/M}$. Similarly, for a given matrix system, fractures propped with multilayers of small-sized proppants have significantly low permeabilities, resulting in a drastic reduction in $PC_{F/M}$.

Fracture-matrix interactions can be further improved by utilizing foam as a mobility control agent, therefore reducing the relative gas permeability within the fracture. (Aboahmed et al., 2023b; Youssif et al., 2024a, 2024b). Typically, foam is a dispersion of gas as a discontinuous phase within networks of liquid films known as lamellae (Kovscek and Radke, 1994). The resilience of foam films serves as a crucial indicator of the effectiveness of the Enhanced Oil Recovery (EOR) process. Increased foam strength and stability lead to greater apparent viscosity and thereby improved interactions between fractures and the surrounding matrix.
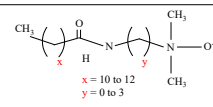
The effectiveness of the foam-based EOR methods in fractured formations has been probed by a few groups in the past (Haugen et al., 2010; Aboahmed et al., 2023b). They showed that the foam plays a pivotal role in reducing the gas mobility in fractures by enhancing its apparent viscosity, thereby retarding its breakthrough (Haugen et al., 2014). This induces the diversion of gas from the fracture toward a previously inaccessible oil-filled matrix (Zhu et al., 1998; Enick et al., 2012; Simjoo et al., 2013; Roncoroni et al., 2021), resulting in improved oil production. Additionally, numerous methods have been proposed in the literature to initiate foam generation in porous media (Saint-Jalmes, 2006; Singh and Mohanty, 2014, 2015; Risal et al., 2019; Wang and Mohanty, 2021; Le Van et al., 2022, 2024; Aboahmed et al., 2023a) contingent upon several parameters such as reservoir conditions, operational factors, surfactant formulations, and oil recovery goals (Youssif et al., 2023). However, these works did not examine the effect of permeability contrast in fractured porous systems.

Generally, foam can be formed either in situ at reservoir conditions or can be pre-generated at the surface and later injected into the porous medium. In situ-generated foam in open fractures is observed to be weak and less efficient in promoting interactions between fracture and matrix via gas diversion to the latter (Kovscek et al., 1995; Haugen et al., 2012). However, introducing proppants into the fractures can lead to solutions that can overcome such challenges. Propped fractures with specific permeability facilitate foam generation due to enhanced snap-off of bubbles from the pore space of the porous medium. Examples from the literature show that permeability plays a crucial role in controlling foam behavior. In addition, the foamability of a surfactant and stability of the aqueous films improve in a specific range of fracture permeability. The bubble generation process encounters serious challenges below and above this critical range, resulting in poor foam performance due to rapid coale-

Table 1. Synthetic brine composition with 20% salinity.

Salt	Concentration (wt.%)
NaCl	13.805
$MgCl_2$	0.492
$CaCl_2$	4.556
Na_2SO_4	0.012
$SrCl_2$	0.239
KCl	0.894
$BaCl_2$	0.003

Table 2. Structure and physical properties of the amphoteric surfactant utilized in this study at 25 °C (Piri et al., 2023).

Structure	MW (g/mol)	Viscosity (mPa.s)	Density (g/cm^3)	CMC[a] (ppm)
	307	45	0.99	300

Notes: [a] CMC denotes the critical micelle concentration of the amphoteric surfactant in 200,000 ppm brine salinity.

scence (Turta and Singhal, 2002). On the other hand, pre-generated foam experiences a substantial change in its physical properties during the injection into the subsurface under elevated pressure and temperature conditions. In such a scenario, the foam texture becomes distinctly dissimilar from that initially generated at the surface because of significant lamella drainage, resulting in dismal foam behavior.

In the present study, we investigate the effect of fracture-matrix permeability contrast on in-situ foam behavior in fractured cores at elevated pressure and temperature conditions. The experiments were performed at operation conditions representative of an unconventional reservoir in North America. To the best of our knowledge, there exists only one example in the literature that examined the impact of permeability ratios on foam performance in unpropped fractured samples (Haugen et al., 2010). In the available study, the permeability ratios were altered using different types of cores with varying matrix permeabilities. The results indicated that the maximum oil recovery was achieved at the lowest permeability ratio. However, the underlying reasons for such behavior remain unclear, and the optimal range of $PC_{F/M}$ within which the foam strength and stability become predominant is yet to be understood. The relationship between permeability contrast and oil recovery is intricately controlled by the factors that regulate foam generation in complex porous media. Determining the ideal $PC_{F/M}$ range is critical for understanding and taming the bubble coalescence dynamics, which, in turn, impact the efficacy of foam in the adverse wetting and morphological conditions of fractured systems. Different from the existing example, the present study employs silica proppants of diverse sizes to create fractures of varying permeabilities. Addition-

ally, it utilizes the same type of rock samples as matrices, which diminishes the possibility of incurring experimental artifacts due to varying petrophysical properties belonging to different kinds of rocks. It should be noted that this approach distinctively highlights the effect of matrix-fracture permeability contrast on oil recovery.

2. Materials and methods

2.1 Fluids

A light crude oil from an unconventional reservoir in North America was utilized in all experiments. It was used to age the core samples to alter their wettability and establish the initial oil saturation in fractures. The oil density and viscosity were 0.7876 g/cm^3 and 0.7701 cP, respectively, at the experimental conditions of 3,500 psi and 115 °C. In addition, industrial-grade methane (CH_4) with a purity of 99.9%, purchased from Air Gas Company, was employed as the foaming gas. The aqueous solutions of the surfactants were prepared in a synthetic brine of 200,000 ppm salinity with a composition representing the formation brine from the selected unconventional reservoir in the United States (see Table 1).

An amphoteric surfactant consisting of a blend of lau-ramidopropylamine and myristamidopropyl amine oxides was utilized as the foaming agent. The selection of this chemical was informed by the results from previous studies, which highlighted its superior foaming performance, particularly under harsh operating and wetting conditions (Le Van et al., 2023; Piri et al., 2023; Youssif et al., 2024b). More details about its molecular structure and properties are provided in Table 2. The aqueous solutions were prepared by dissolving a fixed concentration (6,000 ppm) of this chemical in synthetic brine. The adsorption of surfactant molecules onto carbonate and quartz was investigated elsewhere, confirming their low binding affinity to the surfaces of such grains. Additionally, the results showed that the emulsion formation tendency of this chemical was minimal as they consistently remained in the aqueous phase during the screening tests (Youssif et al., 2024a). Therefore, this amphoteric surfactant emerged as an excellent candidate, capable of generating stable and strong foam in the presence of oil and under the experimental conditions of this study.

2.2 Rock samples and proppants

Four core samples (1 inch in diameter and 10 inches in length) were drilled from blocks of Minnesota Northern Cream Buff (MNCB) acquired from Vetter Stone. They exhibited a notable degree of mineral heterogeneity, including dolomite limestone, calcite, quartz, and traces of other minerals, such as feldspars, kaolinite, gypsum, and pyrite (Youssif et al., 2024b). The porosity and permeability of the matrix core samples ranged between 11% to 14% and 0.5 to 3 millidarcy (mD), respectively. Table 3 describes the physical properties of MNCB rock samples including length (L), diameter (D), porosity (φ), absolute permeability (K), pore volumes (PVs), and initial water saturation (S_{wi}). Silica-based proppants of varying mesh sizes, procured from Magnolia Frac Sand, LLC, were used to prop the fractures.

Table 3. Physical properties of the carbonate core samples used in this study.

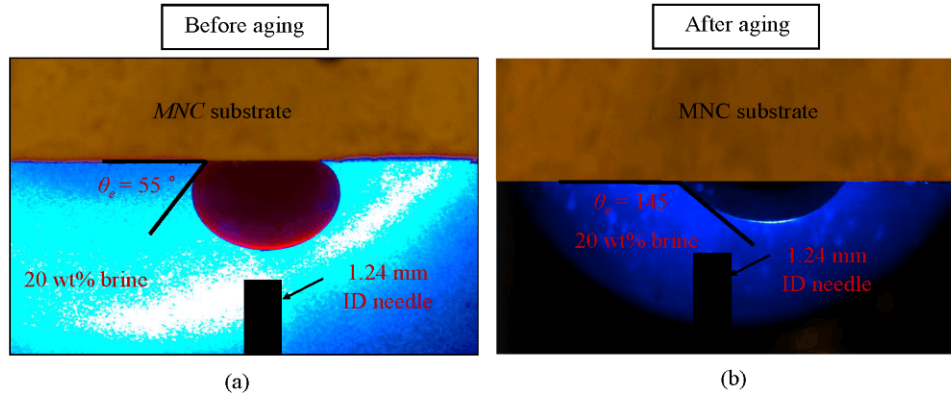| Core plug ID	L (cm)	D (cm)	φ (%)	K (mD)	PVs (cm^3)	S_{wi} (%)
MNCB1	26.01	2.41	14.3	2.4	18.4	10.3
MNCB2	26.05	2.41	14.3	2.8	19.7	12.9
MNCB3	25.78	2.41	12.6	2.8	17.6	12.2
MNCB4	25.79	2.41	15.4	2.6	19.6	15.2

Fig. 2. Measurements of the contact angle between oil droplets and MNCB chips at 3,500 psi and 115 °C show a shift from (a) water-wetness to (b) oil-wetness after static aging.

2.3 Preparation of the core plugs and proppants

Fractures were induced by cutting the whole core samples into two halves along the longitudinal axis using a diamond horizontal saw. Sawed samples were then rinsed with water to remove any residues or contaminants from their surfaces and dried for 48 hours in an oven at 80 °C. The fractured specimen's dry weight was measured as W_1. Subsequently, fractured plugs were vacuum-saturated with crude oil, and the saturated weight was determined (denoted as W_2). These oil-filled fractured core samples were then placed into imbibition cells containing synthetic brine with a salinity of 200,000 ppm, allowing a specific amount of brine to be spontaneously imbibed into the sample matrices. This resulted in an initial water saturation of 10%-15% within the sample matrices (refer to Table 3). The new weight after spontaneous imbibition was estimated as W_3. The pore volume of the matrix (V_p), brine volume (V_w), and oil volume (V_o) were subsequently calculated using the following equations:

$$V_p(cc) = \frac{W_2 - W_1}{\rho_o} \tag{1}$$

$$V_w(cc) = \frac{W_3 - W_2}{\rho_w - \rho_o}, \quad S_w = \frac{V_w}{V_p} \times 100\% \tag{2}$$

$$V_o(cc) = V_p - V_w \tag{3}$$

where ρ_o and ρ_w are the densities of oil and brine in gm/cc, respectively, and S_w is brine saturation in the matrix pores in percentage.

After establishing the oil and brine saturation in the matrix, an aging process was then conducted to alter their wettability from water-wet to oil-wet conditions. To this end, they were placed in a pressure cell filled with crude oil under high-pressure and high-temperature conditions (1,000 psi and 120 °C) for 4 to 6 weeks. Upon completion of the aging process, several chips were taken from the aged samples, and contact angle measurements were conducted on them using the pendant drop method. The results showed that the average contact angle between oil and the aged MNC samples was 145°, as shown in Fig. 2, indicating a significant wettability shift towards strongly oil-wet conditions.

On the other hand, four mixtures (denoted as M_1-M_4) were prepared using proppants of different mesh sizes (20/40, 40/70, 100 and > 300) to create fractures of distinct permeabilities. The blends included 89 wt% of 20/40 and 11 wt% of 40/70 mesh sand (M_1), 50 wt% of 40/70 and 100 mesh sands (M_2), 100 wt% of 100 mesh sand (M_3), and finally, 100 wt% of 300 mesh sand (M_4). These proppants are commonly employed in hydraulically fractured reservoirs. The varying compositions of mixtures with different sizes led to the propped fractures possessing specific pore geometries and, thus, permeabilities. The wettability of the originally water-wet proppants was altered to oil-wet condition using the static aging process. To this end, they were first saturated with 200,000 ppm brine for two to three days and then dried using delicate wipes, which removed excess water. Afterward, the water-saturated sand was loaded into oil-filled accumulators, which were then housed in a conventional oven and pressurized to 1,000 psi. Subsequently, the oven temperature was raised to 120 °C. Upon completion of the aging process, which continued for 10 to 12 weeks, samples of aged sand were collected for wettability characterization. Fourier-transform infrared (FTIR) spectra (see Fig. 3(b)) conducted on the samples of aged 300
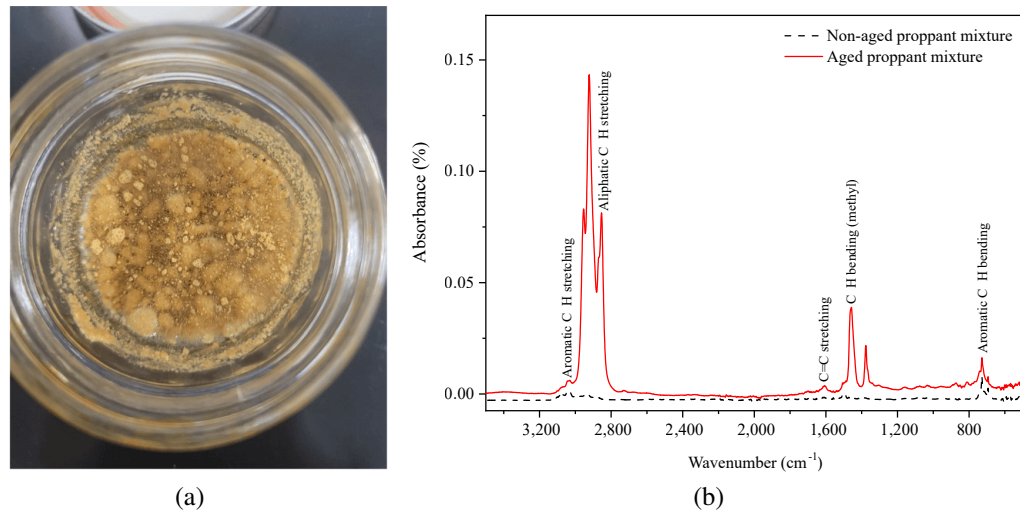
Fig. 3. Characterization of oil-wet proppants of 300 mesh grain size: (a) Visualization photo and (b) FTIR spectra.
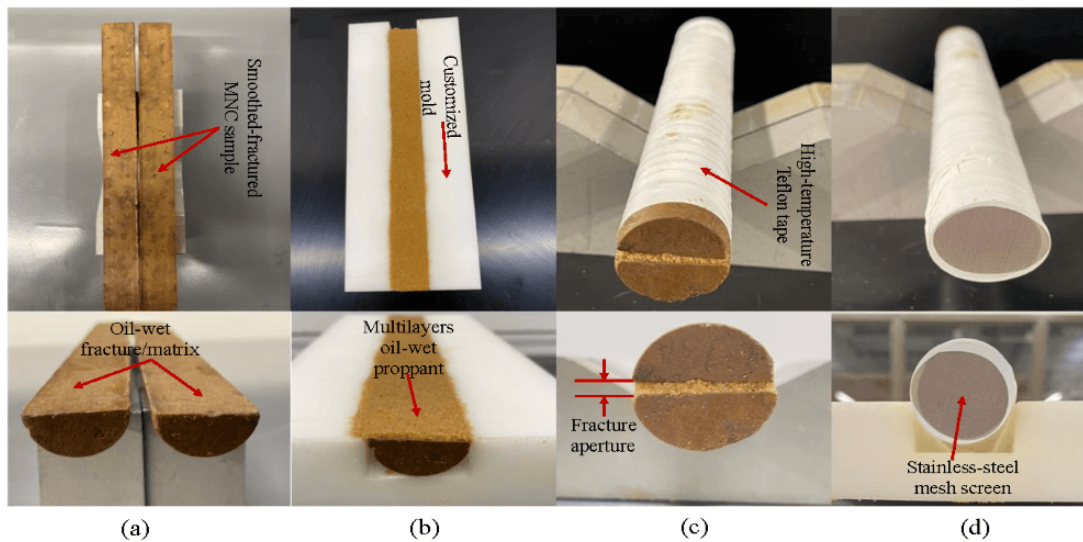

Fig. 4. Typical procedure for preparing a propped fractured MNC core sample. (a) Oil-wet fractured specimen, (b) distribution of multilayers of oil-wet proppant on one of the halves, (c) sandwich-like assembly of both halves wrapped with Teflon tape and (d) propped fractured core assembly enclosed in heat shrink tube and secured using metal screen mesh from both sides.

mesh sand show the adsorption of surface-active species of oil on the proppant surfaces, confirming the wettability alteration from water-wet to oil-wet conditions. The snapshot shown in Fig. 3(a) distinctly demonstrates the separation of oil-wet proppant grains from the brine solution, forming clogs.

2.4 Preparation of proppant-packed fractured samples

The fractured core samples were meticulously propped with the aged sand mixtures following the steps outlined below in Fig. 4. This standard packing procedure ensured a consistent and even distribution of proppants across the fracture surfaces. To this end, the two halves of the oil-wet core sample were positioned horizontally on a customized mold, as shown in Fig. 4(a). A homogeneous layer of oil-wet proppants, with an approximate height varying between 1.1 to 1.4 mm, was formed on top of the surface of one piece (see Fig. 4(b)). Afterward, the second half of the core sample was placed atop the proppant layer, creating a sandwich-like configuration of the entire assembly, which was then wrapped with Teflon tape (see Fig. 4(c)). Finally, it was enclosed within a heat shrink tube, and both ends were secured with metal screens of specific mesh, smaller than the sizes of the proppants packed inside the fractures (Fig. 4(d)).

2.5 Core flooding setup

A three-phase core flooding system, developed in-house, was employed to generate foam and evaluate its performance under the experiment conditions of 115 °C and 3,500 psi. The schematic diagram of the setup is presented in Fig. 5 and is based on a patented three-phase core flooding sys-
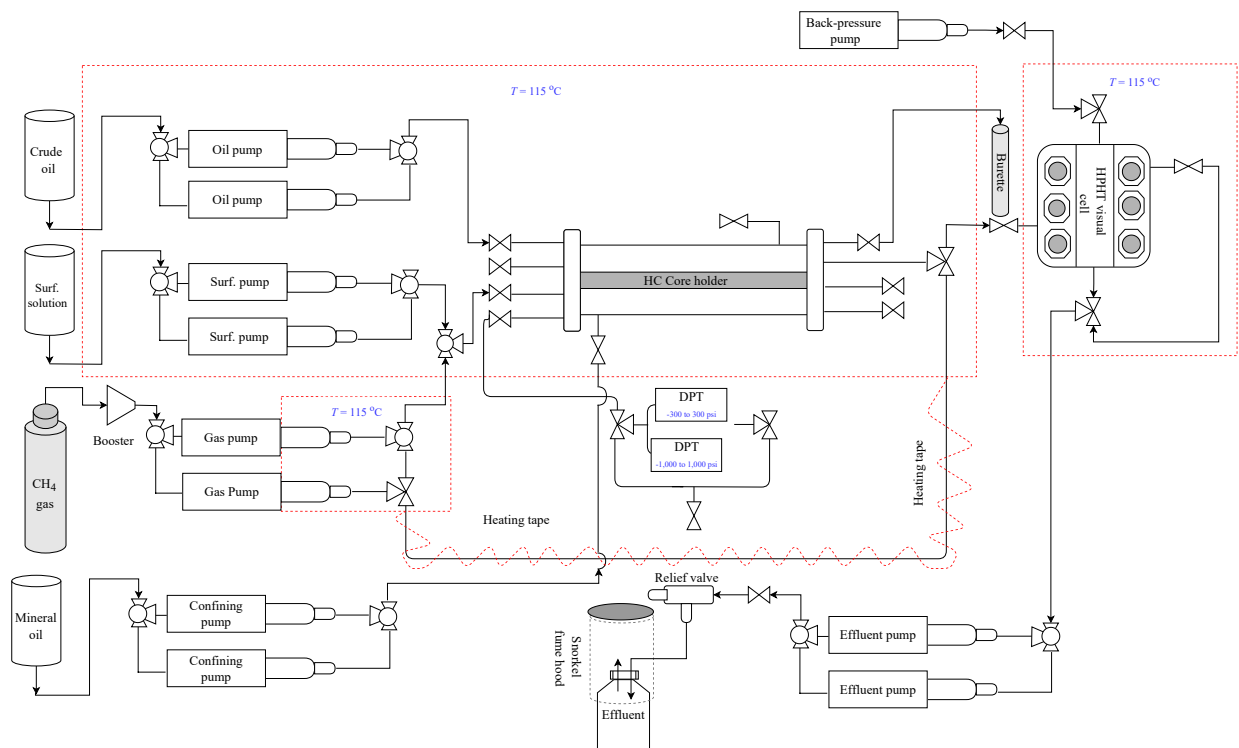
Fig. 5. Schematic diagram of the three-phase macro-scale core flooding apparatus (Youssif et al., 2024a).

tem (Piri, 2014). It consisted of several Quizix precision pumps, a hassler-type core holder, two conventional ovens, pneumatic Vindum valves, a 700-cc Hastelloy pressure cell, differential pressure transducers, a 50-cc visual cell, and flow lines, with all wetting components made of high-pressure and high-temperature compatible Hastelloy material. Specifically, it comprised two dual-cylinder Quizix 6000 series pumps that maintained constant back pressure and introduced methane into the fractured core plugs at specific flow rates. Multiple dual-cylinder Quizix 5000 series pumps were used to inject the nonaqueous (oil) and aqueous phases (brine and foaming agents). Another similar pump imposed an overburden pressure of 4,000 psi on the AFLAS sleeve surrounding the core plug. Furthermore, the Hastelloy fluid lines connecting the gas pumps to the core flooding system were maintained at experimental temperature. To this end, heating tapes were used and covered with insulating material and aluminum foils to minimize heat dissipation. Effluents from the core sample were collected and recorded in an HPHT visual cell operating under experimental conditions. The cell was equipped with a sapphire glass window, which facilitated visual assessment of the produced fluids and volumetric measurements. Additionally, another set of Quizix 5000 series pumps, connected to the bottom of the visual cell, aided in the retraction of fluids under ambient conditions. Pressure transducers with three different ranges, including 0-250 inch-H_2O, 0-300 psi, and 0-2,000 psi, were incorporated into the system to record the pressure gradient across the core samples.

2.6 Experimental procedure

For each experiment, the propped fractured core sample was horizontally loaded into a Hastelloy core holder, and an initial confinement pressure of 500 psi was applied using a manual hand pump. Subsequently, the core holder was placed horizontally in a conventional oven. The propped-fractured core sample was flushed with ethane briefly to remove air and other contaminants and then vacuum-saturated with crude oil for a short period. Initial estimations of the petrophysical properties, including pore volume and porosity of the propped fractures, were then performed. Afterward, the confining pressure and pore pressure were gradually increased using 5000 series Quizix pumps to the experimental conditions of 3,500 and 4,000 psi, respectively. It is noteworthy that the system was fully pressurized with crude oil up to the production line. Concurrently, the 6000 series Quizix back-pressure pump pressurized the visual cell and compartment lines with gaseous methane to 3,500 psi instead of a common dome-loaded back-pressure regulator. This enabled us to maintain a constant back pressure, even at very high flow rates, resulting in a stable equilibrium between the phases. Once the entire system equilibrated at 3,500 psi, the pneumatic Vindum valve separating the production line from the core holder and the production line connected to the visual cell was opened. The oven temperature was then gradually increased to 115 °C, and the system was allowed to stabilize for two days. The absolute permeability of the propped fracture was measured by monitoring the pressure gradient across the fracture using a 0-250 inch-H_2O differential pressure transducer by varying oil flow rates, ranging from 0.5 to 2 cm^3/min, using Darcy's

Table 4. Experimental design and flow parameters used during Phases I-IV of the flooding tests.

Phase	Core plug ID	Proppant mixture	Surfactant concentration in brine (ppm)	Gas flow rate (pre-foam) (cm^3/min)	Foam flow rate (cm^3/min)	Foam quality (%)	Gas flow rate (post-foam) (cm^3/min)
I	MNCB1	M_1	6,000	0.5-6	0.2-3	85	3
II	MNCB2	M_2	6,000	0.5-2	0.2-1.5	85	2
III	MNCB3	M_3	6,000	0.5-2	0.2-1.25	85	2
IV	MNCB4	M_4	6,000	0.5-2	0.02-0.6	85	2

law (Lake, 1989; Johns, 2004), as shown in Eq. (4):

$$\frac{Q_o}{A_f} = \frac{K}{\mu_o} \frac{\Delta P}{L_f} \qquad (4)$$

where Q_o is the oil flow rate in cm^3/s, A_f is the fracture's cross-sectional area in cm^2, μ_o is the oil viscosity in cP, ΔP is the pressure gradient across the fracture in atm, L_f is the fracture length in cm, and K is the absolute permeability of the fracture in Darcy.

Core flooding experiments were conducted on four fractured MNCB cores individually propped with four different mixtures at a pore pressure of 3,500 psi and an overburden pressure of 4,000 psi, resulting in a net confining pressure of 500 psi. Each experiment involved a new core sample to ensure the same initial conditions. The experiments were conducted on fractured MNCB1, MNCB2, MNCB3 and MNCB4 core samples containing mixtures M_1, M_2, M_3 and M_4, respectively (see Table 4 for detail). The following steps were adopted for each experimental phase: (1) pre-foam gas injection, (2) foam flooding and (3) post-foam gas injection.

2.6.1 Pre-foam gas injection

Gaseous methane was injected into the oil-saturated fractures at varying flow rates, from 0.5 to 6 cm^3/min, until no further oil was produced. The pressure drop across the sample was monitored in real-time during the injection, and the cumulative oil recovery was recorded after completing the injection at each flow rate. In principle, the pre-foam gas injection was applied to establish an initial oil saturation condition in the fractures before foam flooding. It is evident from the literature that oil has a detrimental impact on foamability and foam stability (Nikolov et al., 1986; Aveyard, 1993; Farzaneh and Sohrabi, 2013; Yao et al., 2018; Le Van et al., 2023), and reducing its saturation below a critical threshold in the porous medium provides a favorable environment for foam generation.

2.6.2 Foam flooding

The foam injection step was initiated after establishing the initial oil saturation (S_{oi}) within the propped fracture. The foam was generated in situ inside the fractures via simultaneous injection of methane and surfactant solution. This process continued until a steady-state pressure drop was achieved across the core sample, and no further oil recovery from the matrix was observed. All the operational parameters utilized during each phase are listed in Table 4. The pressure gradient profiles across the core sample and the incremental

oil recovery due to foam injection were recorded in real-time. Three key parameters were determined to quantify the foam performance, including the foam's apparent viscosity (μ_f), the mobility reduction factor (MRF), and the oil recovery. The μf was calculated using Eq. (5), derived from Darcy's law considering single-phase flow through the fracture (Simjoo et al., 2013; Clarke et al., 2016; Mitchell et al., 2016):

$$\mu_f = K_{f-o} \frac{A_f}{Q_g + Q_l} \frac{\Delta P_{\text{foam}}}{L} \qquad (5)$$

Whereas MRF was estimated from the ratio of the steady-state pressure drops during foam flooding (ΔP_{foam}) to that observed due to the co-injection of methane and brine in the absence of surfactant ($\Delta P_{\text{no foam}}$), as indicated in Eq. (6) (Mannhardt et al., 1998; Solbakken, 2001; Aarra et al., 2014; Ibrahim et al., 2017):

$$\text{MRF} = \frac{\Delta P_{\text{foam}}}{\Delta P_{\text{no foam}}} \qquad (6)$$

2.6.3 Post-foam gas injection

After concluding the foam flooding, several pore volumes of gaseous methane were injected at a constant flow rate under experimental conditions. The primary objective of this step was to purge the fractures and evaluate the efficacy of gas injection in displacing more oil from the matrix after the foam flooding. As indicated in Table 4, the flow rate during the post-foam gas injection varied based on the fracture configurations of the respective experiment.

3. Results and discussion

This section presents and discusses the results of the three-phase macroscale foam flooding experiments in propped fractured oil-wet core samples. The findings from this study offer crucial insights into the effect of fracture-matrix permeability contrast ($PC_{F/M}$) on foam performance. Different proppant compositions allowed fractures to possess varying permeabilities, from 0.2 to 180 D. First, we show the fracture permeability measurements for all four proppant mixtures using Darcy's law. Subsequently, we estimate the initial oil saturation (S_{oi}) in the fracture due to gas injection prior to foam flooding. Next, the results of foam flooding in propped fractured core samples at varying fracture permeabilities are analyzed. Its impact on the foam performance of the amphoteric surfactant is evaluated carefully and quantified in terms of the foam's apparent viscosity (μ_f), MRF, and oil recovery
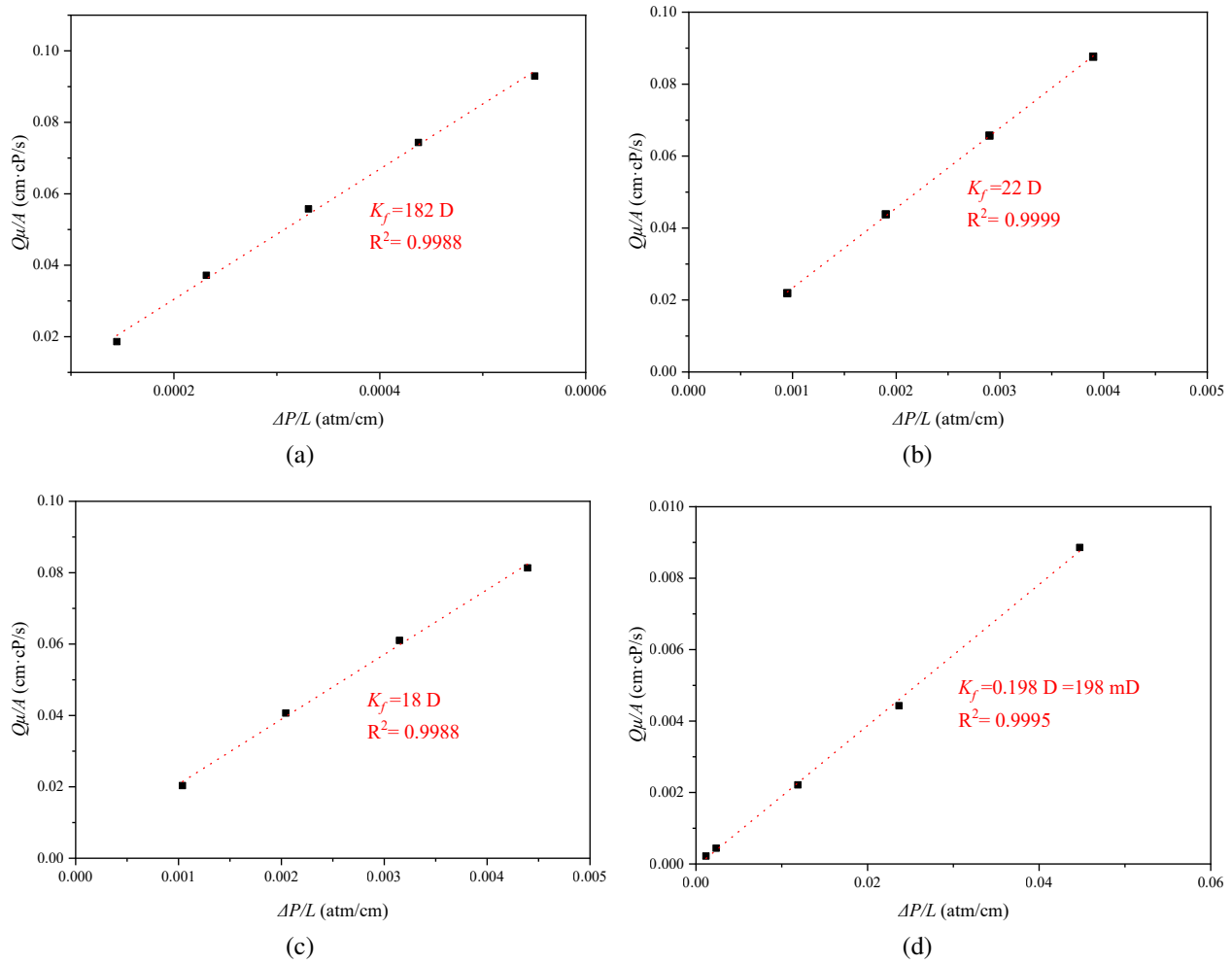
Fig. 6. Absolute permeabilities of the propped fractures at 3,500 psi and 115 °C for proppant with different mesh sizes: (a) 89 wt% of 20/40 mesh-11% wt% of 40/70 mesh (M_1), (b) 50 wt% of 40/70 mesh-50 wt% of 100 (M_2), (c) 100 wt% of 100 mesh (M_3) and (d) 100 wt% of 300 mesh (M_4).

from the matrix.

3.1 Fracture-matrix permeability contrast

The experimentally-measured absolute permeability of propped fractures at the pressure and temperature conditions of 3,500 psi and 115 °C are shown in Fig. 6. The permeabilities were determined by fitting the steady-state pressure gradient data and the corresponding injection rates of crude oil to Darcy's equation. The results from the tests conducted on all four sand mixtures indicated a direct relationship between proppant size and the permeability of the fracture. As evident, fractures packed with larger proppants possessed higher permeabilities, which is attributed to the formation of capillary openings of significant sizes due to the packing of bigger grains. These findings align well with the examples presented in the literature (Zheng et al., 2017; Ramlan et al., 2021). In other words, the grain size distribution of proppants plays a crucial role in controlling the permeability of the fracture, thereby contributing significantly to its conductivity and oil recovery from the neighboring matrix (Ramlan et al., 2021;

Li and Huang, 2022; Skopintsev et al., 2022).

The $PC_{F/M}$ of proppant mixtures M_1, M_2, M_3 and M_4 were calculated to be 7.53E4, 7.94E3, 6.35E3 and 56, respectively, as shown in Fig. 7. Such a broad range of $PC_{F/M}$ facilitates the development of a more accurate understanding of fracture-matrix interactions vis-à-vis the effect of permeability contrast on the local pressure field and subsequent mass transfer with the matrix. In scenarios with very high contrast, e.g., a system with open fracture and a very tight matrix, the invading fluids, for example, gas, mainly flows through the former and exhibit minimal mass transfer with the latter (Zhu et al., 2004; Janssen et al., 2019a). Specifically, in the case of foams, fractures with apertures or pores falling outside a specific threshold range do not trigger the generation of strong and stable bubbles and fail to induce communication with the matrix. However, such interactions are enhanced with descending permeability contrasts and result in diverting the flow of the displacing fluids into the matrix (Youssif et al., 2023), leading to improved oil production. This is attributed to the controlled
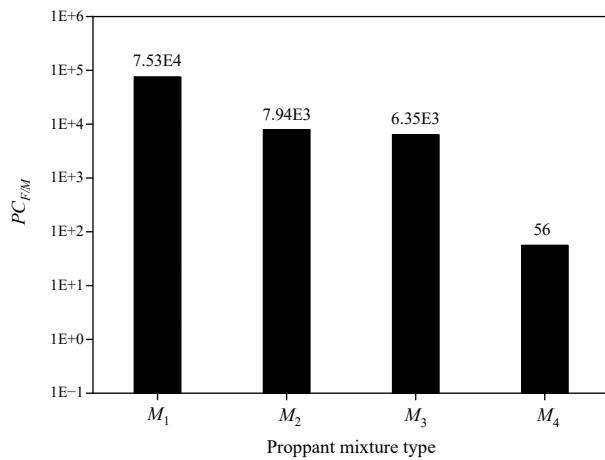
Fig. 7. $PC_{F/M}$ for four proppant mixtures with different mesh sizes.

pores created by packed proppants, which effectively facilitate bubble generation mechanisms such as snap-off and lamella division, thereby improving overall foam performance. However, due to elevated minimum pressure gradients in systems with very low permeability ratios, the efficacy of surfactants in generating strong foam reduces significantly. Therefore, the pressure drop induced by foam must exceed the local threshold pressures of the pores to ensure its flow and stability in the porous medium and prevent it from rapid coalescence and collapse (Rossen, 1990).

3.2 Establishment of the initial oil saturation in fractures

Fig. 8 exhibits the results of cumulative oil recovery from the fracture due to methane injection for all core samples packed with mixtures of different compositions. As the fracture-matrix permeability contrast was reduced, better interactions were expected between the two, improving the oil recovery. The results confirm that the proppant size significantly influenced the interaction dynamics. Specifically, rock sample MNCB1, propped with the largest-sized proppants, exhibited the highest permeability contrast between the fracture and matrix compared to those packed with smaller sizes. As evident from the results shown in Fig. 8, the oil recovery from this sample was lower than that of those with smaller contrasts. This is attributed to the minimal pressure drop observed (0.05 psi) in larger pores of MNCB1, resulting in negligible contact between the fracture and matrix (Zhu et al., 2004; Janssen et al., 2019a). In this case, the oil production is solely from the fracture, and gas mainly invades the larger pores with minimal contact with the oil residing in the smaller ones. Core samples MNCB2 and MNCB3, possessing tighter fractures, displayed slightly higher pressure drops during gas injection, ranging from 0.5 to 0.9 psi, indicating a certain degree of resistance to gas while flowing through the smaller pores in the fracture, displacing more oil as depicted in Fig. 8. It must be noted that this modest pressure drop due to gas-only injection was insufficient to MNCB2 induce fracture-matrix interactions and establish contact with oil-filled pores.

In the case of the lowest permeability fracture (MNCB4),

injecting several pore volumes of methane gas resulted in a notably higher-pressure gradient, as illustrated in Fig. 8. This indicated that gas mobility was relatively reduced while flowing through the tighter pores of the fracture and displacing a significant amount of oil out of the pore space in the fracture and matrix, delaying the gas breakthrough (Sheikha and Pooladi-Darvish, 2009; Kong et al., 2021b). Notably, a considerable portion of the oil was recovered after injecting 2.5 pore volumes of methane. This enhancement stemmed from the improved interactions between the fracture and matrix at the smallest permeability contrast studied in this work. In other words, the gas injection was proven to be relatively efficient in invading the matrix and producing additional oil in the case of a very tight fracture (M_4: packed with 300-mesh proppants). This is attributed to the reduced gas mobility in the fracture, leading to a pressure drop surpassing the local threshold pressure of the matrix pores, which diverts gas from the fracture toward the oil-filled matrix.

3.3 Impact of total flow rate and permeability contrast

Foam generation tests were conducted at ascending flow rates on all four core samples having different fracture permeabilities. The variations in the pressure-time profiles with changes in total flow rate and permeability contrast are shown in Fig. 9. The results demonstrate that the pressure drops due to foam injection increase with shear rate up to a particular value, beyond which the foamability of the chemical becomes insensitive to this variable. It is commonly observed that high shear rates lead to the thinning of the aqueous films, resulting in reduced foam strength and stability. This is attributed to the fact that bubbles formed of weaker lamella become more prone to liquid drainage, diffusion, and coalescence, ultimately leading to poor foam performance.

It should be noted that large pressure drops are expected to occur at significantly high flow rates due to the enforced snapping-off and division of foam bubbles in porous media. In such cases, the foam is generated in large quantities but possesses weak texture, exhibiting rapid diffusion and poor stability. However, it is well understood that the properties of the foaming chemical play a crucial role in withstanding the adverse impact of elevated shear rates on the foam performance. In addition, the results show that the onset of foam generation and foamability of a surfactant in porous media improves at higher injection rates. This is evident by the early occurrence and remarkable pressure gradients observed in the pressure-time profiles presented in Fig. 9.

The results demonstrate that a large population of bubbles per unit volume was generated under such conditions, which is in conformance with the findings presented in the literature (Schramm, 1992; Prud'homme and Khan, 1996; Rossen, 1996). As the pressure surpasses the pore entry value, the lamellae are further stretched, resulting in significant thinning of the aqueous films and eventual deformation of gas bubbles (Pang et al., 2018). Fig. 10 shows the performance in terms of apparent viscosity μ_f and MRF during Phases I to IV of the foam tests conducted at varying flow rates. The results
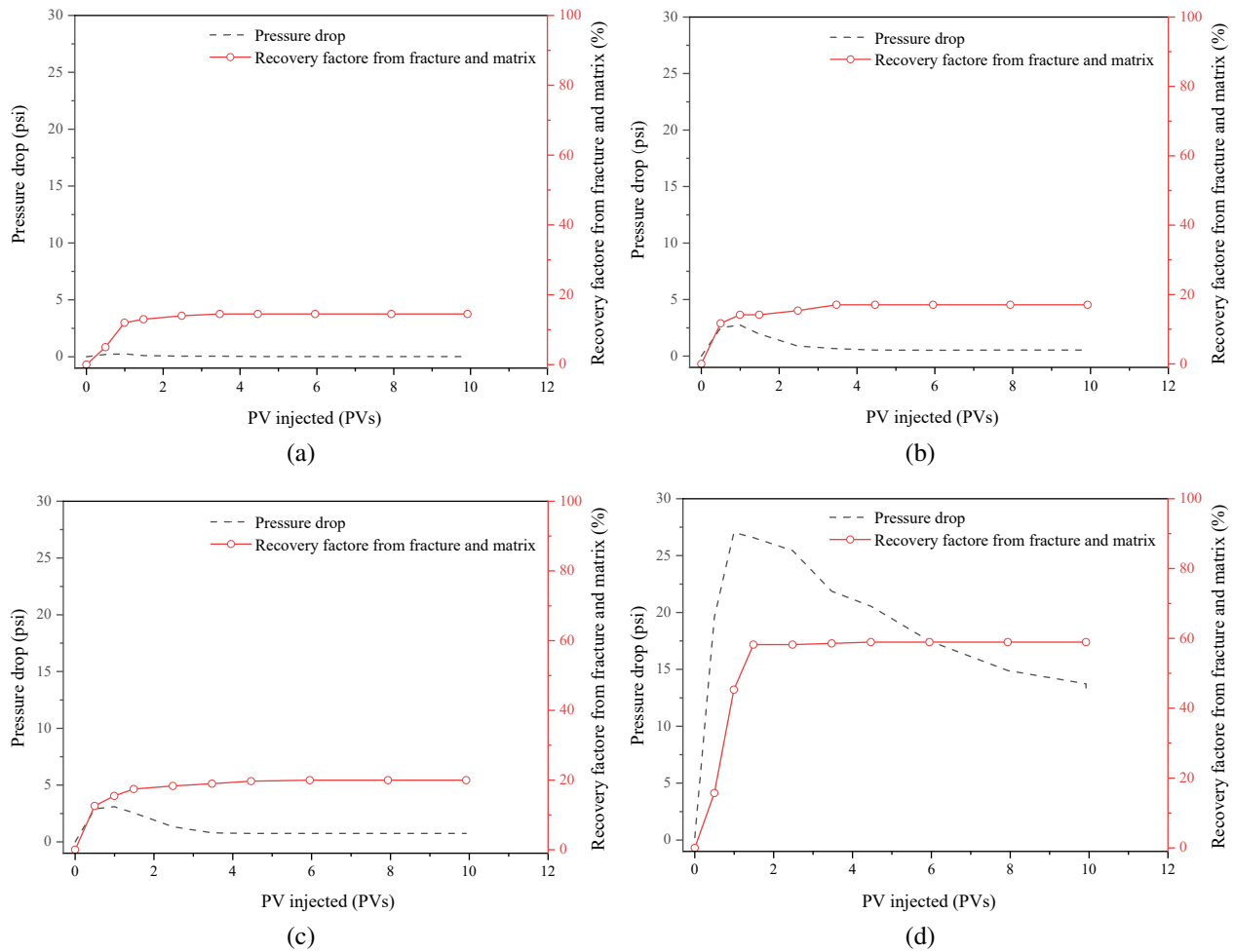
Fig. 8. Cumulative oil recovery and pressure drop profiles during pre-foam gas injection. (a) MNCB1, (b) MNCB2, (c) MNCB3 and (d) MNCB4.

confirm that foam displayed shear-thinning behavior at higher flow rates, as evident by the decreasing apparent viscosities. Despite this fact, large MRF values were observed due to increased pressure gradients induced by foam. Interestingly, a reduction in MRF was witnessed at flow rates above a critical value. Generally, the efficacy of non-Newtonian fluids, such as foam, significantly relies on the degree of heterogeneity within porous media. In our case, the propped fractures serve as a homogeneous medium for foam generation, rendering the shear-thinning behavior of the foam a favorable displacement regime (Xie et al., 2018). On the other hand, as the permeability contrast decreases, foam generation occurs rapidly, even at lower flow rates, leading to elevated pressure drops. As a result, the foam's apparent viscosity was significantly higher in the cases of MNCB2 and MNCB3 ($PC_{F/M}$ of 7.94E3 and 6.35E3) compared to MNCB1 ($PC_{F/M}$ of 7.53E4). This is attributed to the trapping of a significant amount of gas inside the stable lamellae films, resulting in reduced gas mobility (Bashir et al., 2022).

Consequently, more gas was redirected into the tight matrix, leading to a substantial increase in oil production, as demonstrated in Fig. 11. The optimum oil recoveries were

achieved in scenarios with moderate permeability contrasts of 7.94E3 and 6.35E3, outperforming the other two cases with permeability contrasts of 7.53E4 and 56. In the case of the smallest permeability contrast (MNCB4), the foam's apparent viscosity was reduced significantly, causing a drop in oil production from the matrix.

The considerably high-pressure gradient recorded across this sample is attributed to the tightness of the proppant pack within the fracture as well as the foamability of the chemical. The results indicate that a medium with a pore size distribution smaller than a threshold does not facilitate the generation of strong and stable foams. This is because, in a medium with narrow pores, the limiting capillary pressure is surpassed at significantly low foam qualities, i.e., at low to moderate gas saturation conditions. This implies that foam generated at high qualities (85% in our case), which is beyond the transition quality point in such tight systems, suffers from shear thinning and significant bubble coalescence. Therefore, the foamability increases with ascending shear rates but is adversely affected by the rapid collapse of the bubbles due to reduced apparent viscosity, resulting in weak fracture-matrix interactions. Fig. 12 shows the recovery factors from the
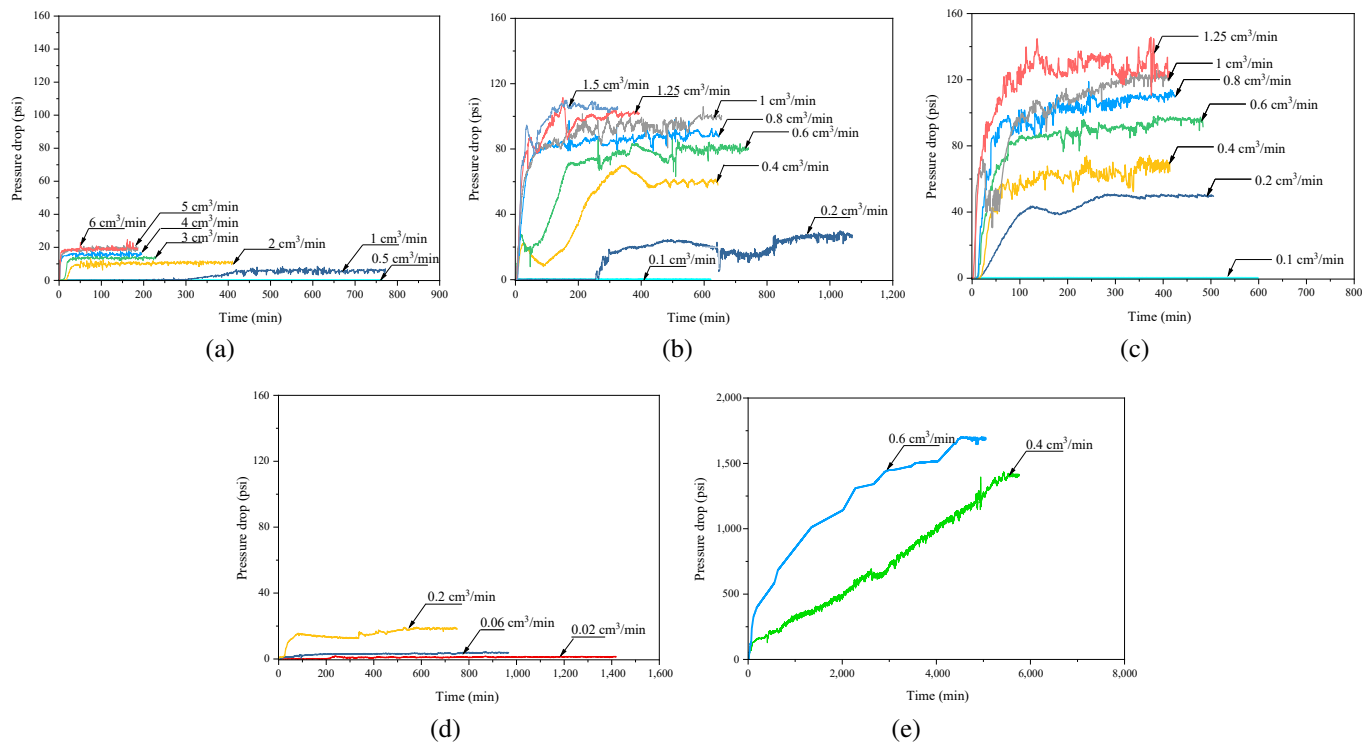
Fig. 9. Pressure drop profiles due to foam injection in all four fractured core samples propped with four different mixtures at varying flow rates and a fixed foam quality of 85%. (a) MNCB1, (b) MNCB2, (c) MNCB3 and (d) and (e) MNCB4.

four propped fractured cores at the end of the foam flooding stage. The results confirm that foam can be more effective in enhancing the fracture-matrix interactions within a specific range of permeability contrast. Notably, the most significant increments in oil recoveries were observed at high to moderate apparent viscosities and not at the largest MRFs (see Fig. 11). This implies that, in cases of varying permeabilities and shear rates, apparent viscosity is a more accurate measure of foam performance than the pressure gradient (i.e., MRF).

3.4 Gas mobility control (post-foam gas injection)

Fig. 13 demonstrates the pressure drop profiles due to gas injection after foam flooding for different durations. In instances where gas injection promptly followed the foam flooding, the gas faced considerable resistance from pre-existing foam within the pore space, as shown in Figs. 13(b) and 13(c). Consequently, it was diverted towards the matrix, facilitating additional oil recovery. This trend was particularly pronounced in all phases except for MNCB1, where the resistance from the generated foam was minimal. In the case of MNCB4, substantial mobility reduction was encountered during the gas injection, as evident by the considerable pressure drop. However, it diminished abruptly due to the relatively weaker foams than that produced in MNCB2 and MNCB3. In the latter cases, the foam persisted for extended durations before collapsing. As a result, these core samples with moderate permeability contrasts (MNCB2 and MNCB3) exhibited an additional oil recovery of approximately 1.53% and 1.66%,

respectively, during post-foam gas injection. This observation conforms to the behavior observed during water-alternating gas processes, wherein the relative permeability of the gas phase diminishes notably while encountering the aqueous phase ahead, compared to gas flooding alone. Consequently, gas fingering is minimized in conditions where the aqueous front leads the gas, resulting in a more steady and uniform displacing-phase front with delayed breakthrough (Afzali et al., 2018, 2020; Kong et al., 2021a). Similarly, the foam acts as a stable displacing system that reduces gas relative permeability within the fracture, inducing its flow towards the matrix and thus improving sweep efficiency. However, it should be noted that this effect is efficient only when a stable foam front is present, as demonstrated in the cases of MNCB2 and MNCB3. After foam flooding, the foam generated within the fracture gradually dissipated over time, resulting in a decreased resistance encountered by the injected gas. Hence, it can be stated that the efficacy of post-foam gas injection is more effective when conducted immediately after foam flooding in the systems with moderate fracture-matrix permeability contrasts.

4. Conclusions and recommendations

This study examined the impact of fracture-matrix permeability contrast on the effectiveness of foam flooding in fractured oil-wet carbonate rocks at reservoir conditions. Fracture permeability was varied using proppants of different grain sizes: coarse (Phase I), medium (Phases II and III), and fine (Phase IV). In each phase, the experiments were conducted in
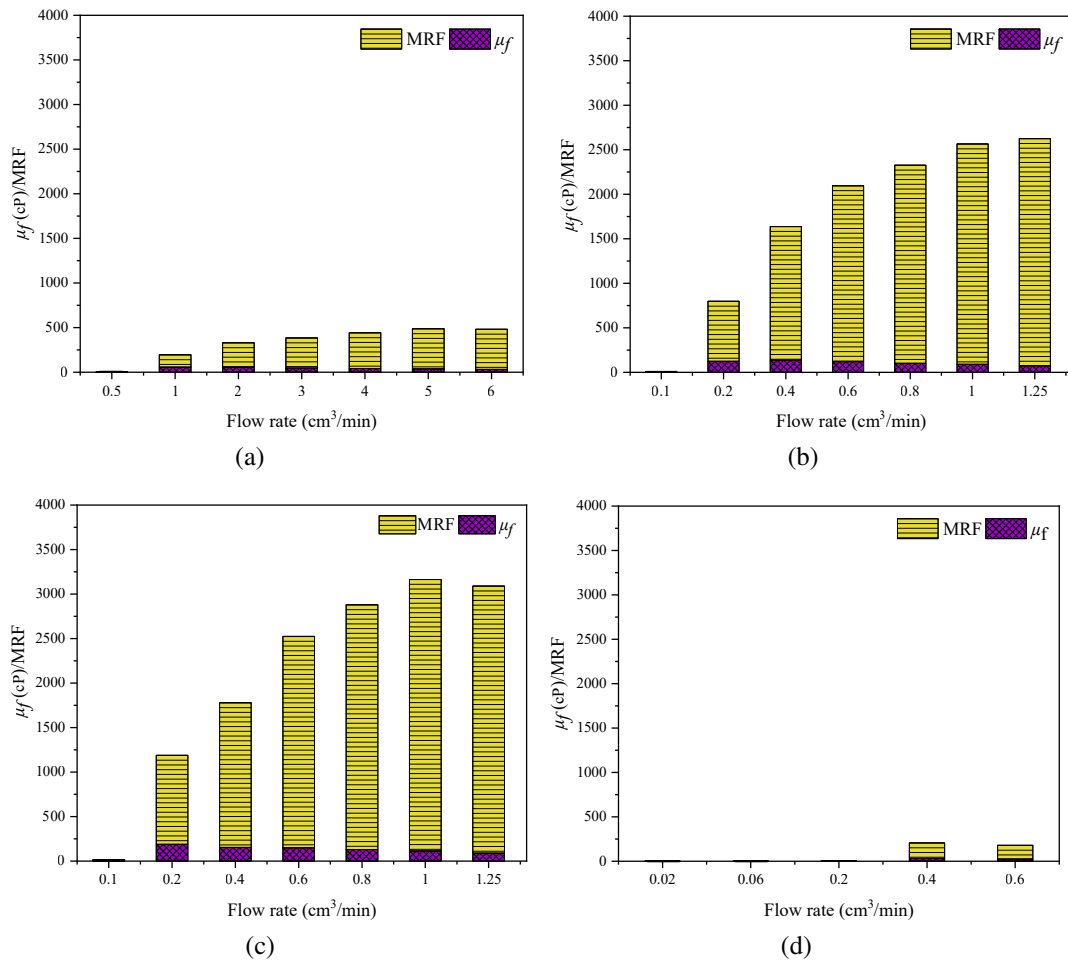
Fig. 10. Variations in the foam's apparent viscosity and MRF with changes in total flow rates and fracture permeabilities. (a) MNCB1, (b) MNCB2, (c) MNCB3 and (d) MNCB4.

three stages: (1) Pre-foam gas injection, (2) foam flooding and (3) post-foam gas injection. The main findings of this study can be summarized as follows. The transmissibility between the matrix and fracture is enhanced with a decreasing contrast between the permeability of the two, highlighting the interplay between permeability and dynamics of fluid flow. The findings revealed that in Phases I-III, pre-foam gas injection resulted in oil production primarily from fractures. However, in Phase IV, characterized by relatively tight proppants' pores, oil was extracted from both fractures and matrix. This is attributed to the improved fracture-matrix interactions due to the elevated pressure gradient across the fracture, which facilitated the invasion of gas into the matrix, thereby sweeping inaccessible oil from these pores.

On the other hand, during foam flooding, the foam's apparent viscosity (μ_f) and MRF increased with the decrease in permeability contrast until reaching a critical threshold value. Beyond this, both parameters experienced a notable decrease due to the instability of gas bubbles. This behavior is ascribed to the foam generated in Phase IV is prone to collapse when lamellae films are further stretched within the porous media due to strong capillary forces. Interestingly, despite

having similar permeability contrasts, the proppant mixtures with a wide range of grain sizes exhibited distinct pore size distributions, leading to significantly different foam behaviors.

The results also indicated that conducting post-foam gas injection promptly resulted in additional oil recovery from core samples packed with medium-sized proppants (Phases II and III). This performance stemmed from the superior stability of the generated foam, which served as a barrier within these fractures. Consequently, gas relative permeability is reduced, and fracture-matrix interactions are enhanced, ultimately leading to increased oil recovery. However, this approach was ineffective in fractures with large and ultra-low permeabilities, i.e., the cases of coarse and fine-sized proppants, respectively. This is attributed to the weaker texture of the foam generated in such systems, rendering it highly susceptible to collapse under the shear forces exerted by gas injections. Therefore, the results suggested that foam is more effective in enhancing fracture-matrix interactions within a specific range of permeability contrast.

The outcomes of this study emphasize the significant relevance of hydrocarbon-based foam flooding to addressing the challenges associated with gas injection in fractured reser-
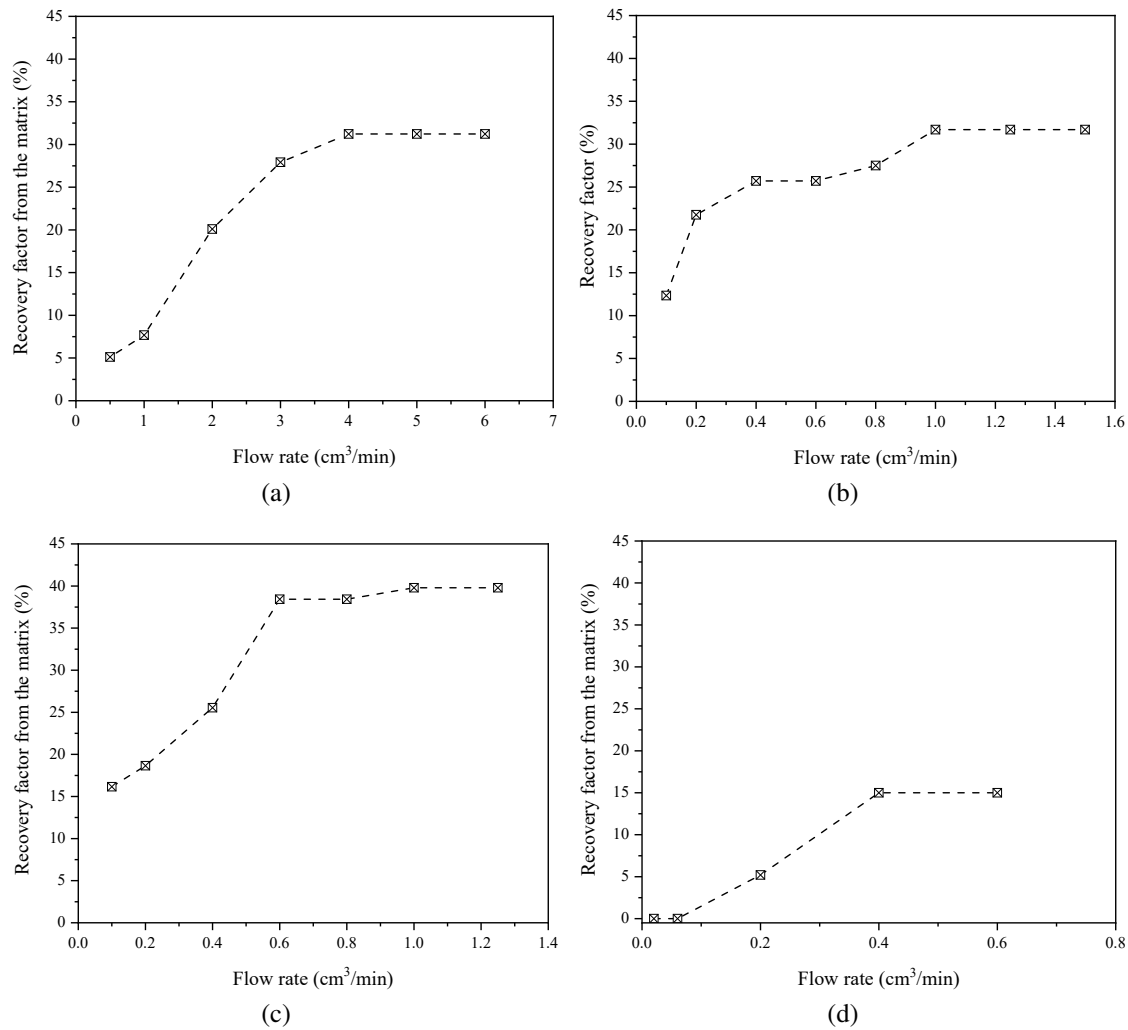
Fig. 11. Variations in the cumulative oil recovery factors in different fractured core samples during foam flooding at varying flow rates. (a) MNCB1, (b) MNCB2, (c) MNCB3 and (d) MNCB4.
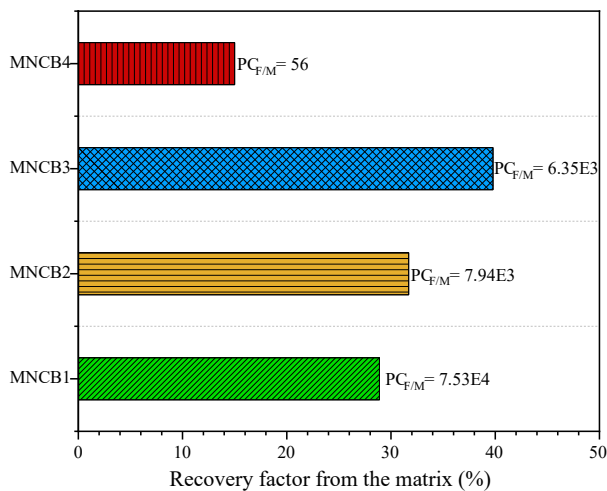

Fig. 12. Recovery factors from the matrices of different core samples at the end of the foam flooding.

voirs. Supported by the findings from this work, foam flooding emerges as a promising scheme for EOR in conventional and unconventional reservoirs within a particular range of fracture-matrix permeability contrast. Moreover, this investigation presents a framework for systemic characterization of the fracture-matrix interactions, which is essential for the successful field-scale deployment of foam-EOR in fractured systems.

Conflict of interest

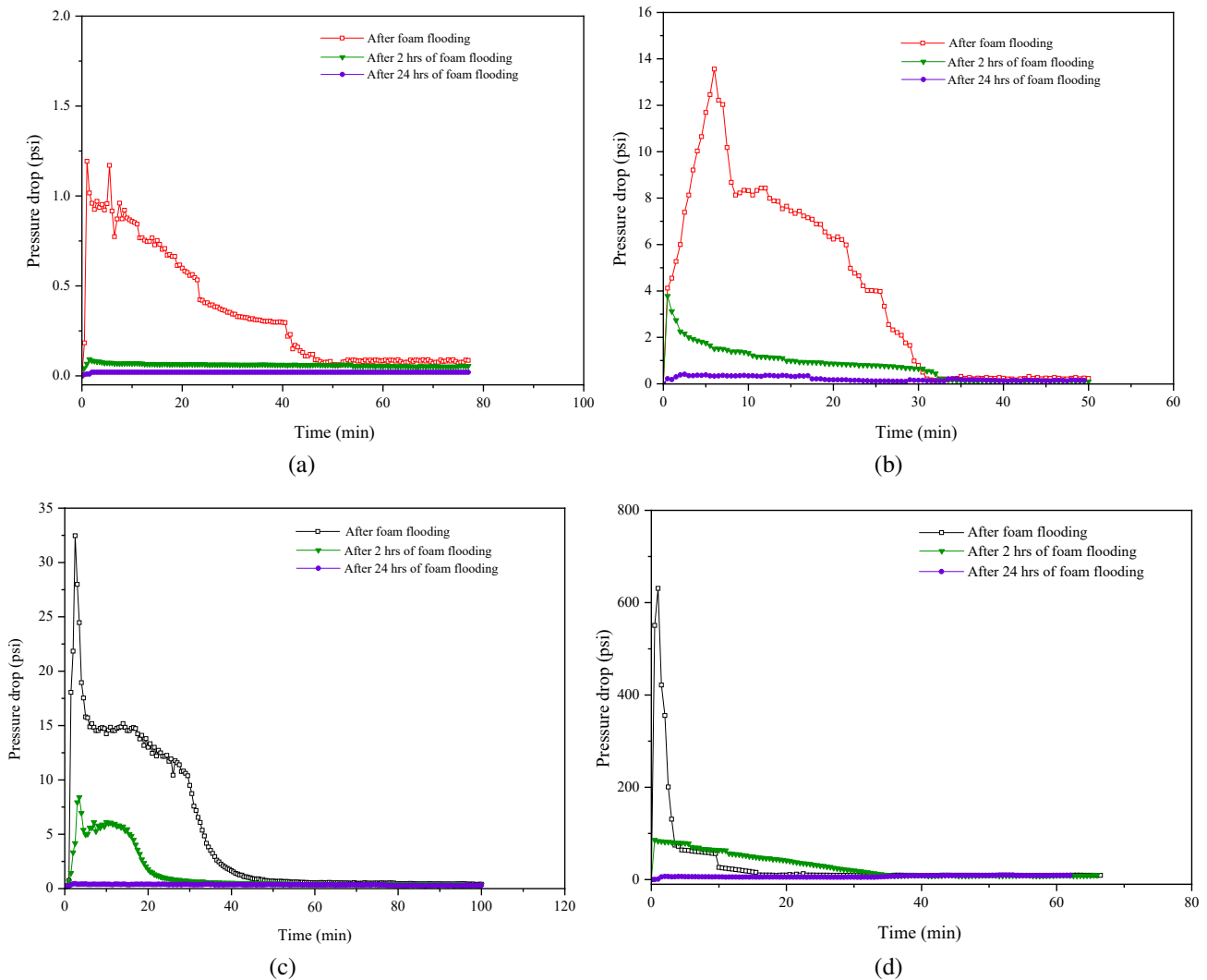The authors declare no competing interest.

Fig. 13. Pressure drop profiles of gas injection obtained after foam flooding for different time durations. (a) MNCB1, (b) MNCB2, (c) MNCB3 and (d) MNCB4.

References

Aarra, M. G., Skauge, A., Solbakken, J., et al. Properties of N_2- and CO_2-foams as a function of pressure. Journal of Petroleum Science and Engineering, 2014, 116: 72-80.

Aboahmed, A. K., Youssif, M. I., Piri, M., et al. Graphene quantum dot-stabilized foam for enhanced oil recovery. Industrial & Engineering Chemistry Research, 2023a, 62(33): 13260-13273.

Aboahmed, A. K., Youssif, M. I., Piri, M., et al. Nanofluid-based foam for enhanced oil recovery in fractured carbonates. Energy & Fuels, 2023b, 37(23): 18772-18784.

Afzali, S., Ghamartale, A., Rezaei, N., et al. Mathematical modeling and simulation of water-alternating-gas (WAG) process by incorporating capillary pressure and hysteresis effects. Fuel, 2020, 263: 116362.

Afzali, S., Rezaei, N., Zendehboudi, S. A comprehensive review on enhanced oil recovery by water alternating gas (WAG) injection. Fuel, 2018, 227: 218-246.

Allan, J., Sun, S. Controls on recovery factor in fractured reservoirs: Lessons learned from 100 fractured fields. Paper SPE 84590 Presented at the SPE Annual Technical Conference and Exhibition, Denver, Colorado, 5-8 October, 2003.

Aveyard, R., Binks, B. P., Fletcher, P. D. I., et al. Entry and spreading of alkane drops at the air/surfactant solution interface in relation to foam and soap film stability. Journal of the Chemical Society, Faraday Transactions, 1993, 89(24): 4313-4321.

Bashir, A., Haddad, A. S. Sherratt, J., et al. An investigation of viscous oil displacement in a fractured porous medium using polymer-enhanced surfactant alternating foam flooding. Journal of Petroleum Science and Engineering, 2022, 212: 110280.

Burchette, T. P. Carbonate rocks and petroleum reservoirs: A geological perspective from the industry. Geological Society, London, Special Publications, 2012, 370: 17-37.

Chen, P., Mohanty, K. Surfactant-enhanced oil recovery from fractured oil-wet carbonates: Effects of low IFT and

wettability Alteration. Paper SPE 173797 Presented at the SPE International Symposium on Oilfield Chemistry, The Woodlands, Texas, USA, 13-15 April, 2015.

Clarke, A., Howe, A. M., Mitchell, J., et al. How viscoelastic-polymer flooding enhances displacement efficiency. SPE Journal, 2016, 21(3): 675-687.

Davidson, D. A., Snowdon, D. M. Beaver river middle devonian carbonate: Performance review of a high-relief, fractured gas reservoir with water influx. Journal of Petroleum Technology, 1978, 30(12): 1672-1678.

Dominguez, G. C. Carbonate Reservoir Characterization: A Geologic-Engineering Analysis, Part I. New York, USA, Elsevier, 1992.

Dordzie, G., Dejam, M. Enhanced oil recovery from fractured carbonate reservoirs using nanoparticles with low salinity water and surfactant: A review on experimental and simulation studies. Advances in Colloid and Interface Science, 2021, 293: 102449.

Elfeel, M. A., Al-Dhahli, A., Geiger, S., et al. Fracture-matrix interactions during immiscible three-phase flow. Journal of Petroleum Science and Engineering, 2016, 143: 171-186.

Enick, R. M., Olsen, D., Ammer, J., et al. Mobility and conformance control for CO_2 EOR via thickeners, foams, and gels-A literature review of 40 years of research and pilot tests. Paper SPE 154122 Presented at the SPE Improved Oil Recovery Symposium, Tulsa, Oklahoma, USA, 14-18 April, 2012.

Farzaneh, S. A., Sohrabi, M. A review of the status of foam applications in enhanced oil recovery. Paper SPE 164917 Presented at the EAGE Annual Conference & Exhibition Incorporating SPE, London, UK, 10-13 June, 2013.

Fernø, M. A. Enhanced oil recovery in fractured reservoirs, in Introduction to Enhanced Oil Recovery (EOR) Processes and Bioremediation of Oil-Contaminated Sites, edited by L. Romero-Zerón, IntechOpen, Rijeka, pp. 89-110, 2012.

Fitch, P. J. R. Heterogeneity in the petrophysical properties of carbonate reservoirs. Leicester, University of Leicester, 2011.

Guerriero, V., Mazzoli, S., Iannace, A., et al. A permeability model for naturally fractured carbonate reservoirs. Marine and Petroleum Geology, 2013, 40: 115-134.

Haugen, A., Fernø, M. A., Graue, A., et al. Experimental study of foam flow in fractured oil-wet limestone for enhanced oil recovery. Paper SPE 129763 Presented at the SPE Improved Oil Recovery Symposium, Tulsa, Oklahoma, USA, 24-28 April, 2010.

Haugen, A., Fernø, M. A., Graue, A., et al. Experimental study of foam flow in fractured oil-wet limestone for enhanced oil recovery. SPE Reservoir Evaluation & Engineering, 2012, 15(2): 218-228.

Haugen, A., Mani, N., Svenningsen, S., et al. Miscible and immiscible foam injection for mobility control and EOR in fractured oil-wet carbonate rocks. Transport in Porous Media, 2014, 104: 109-131.

Ibrahim, A. F., Emrani, A., Nasraldin, H. Stabilized CO_2 foam for EOR applications. Paper CMTC 486215 Presented at the Carbon Management Technology Conference, Hous-

ton, Texas, USA, 17-20 July, 2017.

Janssen, M. T. G., Mutawa, A. S., Pilus, R. M., et al. Foam-assisted chemical flooding for enhanced oil recovery: Effects of slug salinity and drive foam strength. Energy & Fuels, 2019a, 33(6): 4951-4963.

Janssen, M. T. G., Zitha, P. L. J., Pilus, R. M. Oil recovery by alkaline/surfactant/foam flooding: Effect of drive-foam quality on oil-bank propagation. SPE Journal, 2019b, 24(6): 2758-2775.

Johns, R. T. Oil recovery, in Encyclopedia of Energy, edited by C. J. Cleveland, Elsevier Science, Boston, pp. 701-713, 2004.

Karimaie, H., Darvish, G. R., Lindeberg, E., et al. Secondary and tertiary gas injection in fractured carbonate rock: Experimental study. Journal of Petroleum Science and Engineering, 2008, 62(1-2): 45-51.

Karimova, M., Kashiri, R., Pourafshary, P., et al. A Review of wettability alteration by spontaneous imbibition using low-salinity water in naturally fractured reservoirs. Energies, 2023, 16(5): 2373.

Kong, D., Gao, Y., Sarma, H., et al. Experimental investigation of immiscible water-alternating-gas injection in ultra-high water-cut stage reservoir. Advances in Geo-Energy Research, 2021a, 5(2): 139-152.

Kong, D., Lian, P., Zheng, R., et al. Performance demonstration of gas-assisted gravity drainage in a heterogeneous reservoir using a 3D scaled model. RSC Advances, 2021b, 11: 30610-30622.

Kovscek, A. R., Radke, C. J. Fundamentals of foam transport in porous media, in Foams: Fundamentals and Applications in The Petroleum Industry, edited by L. L. Schramm, American Chemical Society, New York, pp. 115-163, 1994.

Kovscek, A. R., Tretheway, D. C., Persoff, P., et al. Foam flow through a transparent rough-walled rock fracture. Journal of Petroleum Science and Engineering, 1995, 13(2): 75-86.

Lake, L. W. Enhanced Oil Recovery. Bergen, USA, Prentice Hall, 1989.

Le Van, S., Sharma, K. V., Hanamertani, A. S., et al. Methane foam performance in oil-wet unconsolidated porous media: A systematic experimental investigation at reservoir conditions. Fuel, 2023, 344: 128002.

Le Van, S., Sharma, K. V., Piri, M. The effects of wettability and permeability on hydrocarbon foam performance in unconsolidated porous media: An experimental investigation at elevated pressure and temperature conditions. Fuel, 2024, 359: 130379.

Le Van, S., Youssif, M. I., Hanamertani, A. S., et al. Methane foam performance evaluation in water-wet unconsolidated porous media: A systematic experimental investigation at elevated pressure and temperature conditions. Journal of Natural Gas Science and Engineering, 2022, 108: 104835.

Liang, F., Sayed, M., Al-Muntasheri, G. A., et al. A comprehensive review on proppant technologies. Petroleum, 2016, 2(1): 26-39.

Li, H., Huang, B. A new permeability model of fracture

containing proppants. Journal of Natural Gas Science and Engineering, 2022, 104: 104661.

Mannhardt, K., Novosad, J. J., Schramm, L. L. Foam/oil interactions at reservoir conditions. Paper SPE 39681 Presented at the SPE/DOE Improved Oil Recovery Symposium, Tulsa, Oklahoma, 19-22 April, 1998.

Mitchell, J., Lyons, K., Howe, A. M., et al. Viscoelastic polymer flows and elastic turbulence in three-dimensional porous structures. Soft Matter, 2016, 12: 460-468.

Moore, C. H., Wade, W. J. Natural fracturing in carbonate reservoirs, in Developments in Sedimentology (Volumn 67), edited by C. H. Moore, and W. J. Wade, Elsevier, New York, pp. 285-300, 2013.

Nikolov, A. D., Wasan, D. T., Huang, D. W., et al. The effect of oil on foam stability: mechanisms and implications for oil displacement by foam in porous media. Paper SPE 15443 Presented at the SPE Annual Technical Conference and Exhibition, New Orleans, Louisiana, 5-8 October, 1986.

Panfili, P., Cominelli, A. Simulation of miscible gas injection in a fractured carbonate reservoir using an embedded discrete fracture model. Paper SPE 171830 Presented at the Abu Dhabi International Petroleum Exhibition and Conference, Abu Dhabi, UAE, 10-13 November, 2014.

Pang, Z., Lyu, X., Zhang, F., et al. The macroscopic and microscopic analysis on the performance of steam foams during thermal recovery in heavy oil reservoirs. Fuel, 2018, 233: 166-176.

Park, H., Park, Y., Lee, Y., et al. Efficiency of enhanced oil recovery by injection of low-salinity water in barium-containing carbonate reservoirs. Petroleum Science, 2018, 15: 772-782.

Piri, M. Recirculating, constant backpressure core flooding apparatus and method. US8683858B2, 2014.

Piri, M., Saraji, S., Hanamertani, A. S., et al. Foaming agents, gas mobility control agents, methods, and systems for enhanced oil recovery. US20230303912A1, 2023.

Prud'homme, R. K., Khan, S. A. Foams: Theory, Measurements and Applications. New York, USA, Routledge, 1996.

Qin, Z., Arshadi, M., Piri, M. Micro-scale experimental investigations of multiphase flow in oil-wet carbonates. I. In situ wettability and low-salinity waterflooding. Fuel, 2019, 257: 116014.

Ramlan, A. S., Zin, R. M., Abu Bakar, N. F., et al. Recent progress on proppant laboratory testing method: Characterisation, conductivity, transportation, and erosivity. Journal of Petroleum Science and Engineering, 2021, 205: 108871.

Rashid, F., Hussein, D., Lorinczi, P., et al. The effect of fracturing on permeability in carbonate reservoir rocks. Marine and Petroleum Geology, 2023, 152: 106240.

Risal, A. R., Manan, M. A., Yekeen, N., et al. Experimental investigation of enhancement of carbon dioxide foam stability, pore plugging, and oil recovery in the presence of silica nanoparticles. Petroleum Science, 2019, 16: 344-356.

Roncoroni, M. A., Romero, P., Montes, J., et al. Enhancement of a foaming formulation with a zwitterionic surfactant for gas mobility control in harsh reservoir conditions. Petroleum Science, 2021, 18(5): 1409-1426.

Rossen, W. R. Minimum pressure gradient for foam flow in porous media: Effect of interactions with stationary lamellae. Journal of Colloid and Interface Science, 1990, 139(2): 457-468.

Rossen, W. R. Foams in enhanced oil recovery, in Foams: Theory, Measurements, and Applications, edited by R. K. Prud'homme and S. A. Khan, Routledge, New York, pp. 413-464, 1996.

Saint-Jalmes, A. Physical chemistry in foam drainage and coarsening. Soft Matter, 2006, 2: 836-849.

Sayedakram, N. I., Mamora, D. Simulation study on surfactant-polymer flood performance in fractured carbonate reservoir. Paper SPE 149106 Presented at the SPE/DGS Saudi Arabia Section Technical Symposium and Exhibition, Al-Khobar, Saudi Arabia, 15-18 May, 2011.

Schramm, L. L. Foams: Fundamentals and Applications in the Petroleum Industry. Washington, USA, Advances in Chemistry, 1992.

Sedaghat, M. H., Ghazanfari, M. H., Parvazdavani, M., et al. Experimental investigation of microscopic/macroscopic efficiency of polymer flooding in fractured heavy oil five-spot systems. Journal of Energy Resources Technology, 2013, 135(3): 032901.

Shafiei, A., Dusseault, M. B., Kosari, E., et al. Natural fractures characterization and in situ stresses inference in a carbonate reservoir-an integrated approach. Energies, 2018, 11(2): 312.

Shedid, S. A. Influences of fracture orientation on oil recovery by water and polymer flooding processes: An experimental approach. Journal of Petroleum Science and Engineering, 2006, 50(3-4): 285-292.

Sheikha, H., Pooladi-Darvish, M. The effect of pressure-decline rate and pressure gradient on the behavior of solution-gas drive in heavy oil. SPE Reservoir Evaluation & Engineering, 2009, 12(3): 390-398.

Simjoo, M., Andrianov, A., Talanana, M., et al. Novel insight into foam mobility control. SPE Journal, 2013, 18(3): 416-427.

Singh, R., Mohanty, K. K. Synergistic stabilization of foams by a mixture of nanoparticles and surfactants. Paper SPE 169126 Presented at the SPE Improved Oil Recovery Symposium, Tulsa, Oklahoma, USA, 12-16 April, 2014.

Singh, R., Mohanty, K. K. Synergy between nanoparticles and surfactants in stabilizing foams for oil recovery. Energy & Fuels, 2015, 29(2): 467-479.

Skopintsev, A. M., Dontsov, E. V., Baykin, A. N., et al. The influence of heterogeneous proppant pack on fracture closure and productivity. Journal of Petroleum Science and Engineering, 2022, 214: 110494.

Sofla, S. J. D., Pouladi, B., Sharifi, M., et al. Experimental and simulation study of gas diffusion effect during gas injection into naturally fractured reservoirs. Journal of Natural Gas Science and Engineering, 2016, 33: 438-447.

Solbakken, J. S. Experimental studies of N_2-and CO_2-foam properties in relation to enhanced oil Recovery applica-

tions. Bergen, University of Bergen, 2001.

Turta, A. T., Singhal, A. K. Field foam applications in enhanced oil recovery projects: Screening and design aspects. Journal of Canadian Petroleum Technology, 2002, 41(10): PETSOC-02-10-14.

Van Golf-Racht, T. D. Naturally-fractured carbonate reservoirs, in Developments in Petroleum Science (Volumn 44, Part 2), edited by Chilingarian, G. V., Mazzullo, S. J. and Rieke, H. H., Elsevier, New York, pp. 683-771, 1996.

Wang, X., Mohanty, K. Improved oil recovery in fractured reservoirs by strong foams stabilized by nanoparticles. Energy & Fuels, 2021, 35(5): 3857-3866.

Xie, C., Lv, W., Wang, M. Shear-thinning or shear-thickening fluid for better EOR? A direct pore-scale study. Journal of Petroleum Science and Engineering, 2018, 161: 683-691.

Yao, X., Yi, P., Zhao, G., et al. A study of the stability mechanism of the dispersed particle gel three-phase foam using the interfacial dilational rheology method. Materials, 2018, 11(5): 699.

Youssif, M. I. In-situ Foam Generation: A superior method for enhanced oil recovery in unconventional fractured reservoirs, in Innovations in Enhanced and Improved Oil Recovery-New Advances, edited by Zoveidavianpoor, M., Intechopen, London, pp. 101-122, 2023.

Youssif, M. I., Sharma, K. V., Goual, L., et al. Experimental evaluation of foam-assisted gas injection in proppant-packed fractured oil-wet carbonate. Energy & Fuels, 2024b, 38(4): 3032-3056.

Youssif, M. I., Sharma, K. V., Piri, M. Hydrocarbon gas foam injection in fractured oil-wet carbonate samples: An experimental investigation of the effect of fracture-matrix permeability contrast on oil recovery. Paper SPE 212736 Presented at the SPE Canadian Energy Technology Conference and Exhibition, Calgary, Alberta, Canada, 15-16 March, 2023.

Youssif, M. I., Sharma, K. V., Shoukry, A. E., et al. Methane foam performance evaluation in fractured oil-wet carbonate systems at elevated pressure and temperature conditions. Journal of Environmental Chemical Engineering, 2024a, 12(3): 112444.

Zaeri, M. R., Hashemi, R., Shahverdi, H., et al. Enhanced oil recovery from carbonate reservoirs by spontaneous imbibition of low salinity water. Petroleum Science, 2018, 15: 564-576.

Zheng, X., Chen, M., Hou, B., et al. Effect of proppant distribution pattern on fracture conductivity and permeability in channel fracturing. Journal of Petroleum Science and Engineering, 2017, 149: 98-106.

Zhu, T., Ogbe, D. O., Khataniar, S. Improving the foam performance for mobility control and improved sweep efficiency in gas flooding. Industrial & Engineering Chemistry Research, 2004, 43(15): 4413-4421.

Zhu, T., Strycker, A., Raible, C. J., et al. Foams for mobility control and improved sweep efficiency in gas flooding improved oil recovery. Paper SPE 39680 Presented at the SPE/DOE Improved Oil Recovery Symposium, Tulsa, Oklahoma, 19-22 April, 1998.